Radial Distribution Functions of Fluid Argon*

Ashfaq A. Khan

Physics Department, University of Florida, Gainesville, Florida

(Received 28 October 1963)

The purpose of the present work is twofold. In the first place, we have deduced from theoretical considerations which of the two integral equations [the Percus-Yevick (PY) and convolution hypernetted chain (CHNC) equations] will yield a better distribution function (g) under different conditions of temperature and density, and for different interaction potentials. In the second place, we have computed the g's of fluid argon at several values of temperature (all below the critical temperature) and density. The computed g's from the PY and CHNC integral equations using the two different interaction potentials (the Lennard-Jones and Guggenheim-McGlashan potentials) between the argon atoms are compared among themselves as well as with the experimental curves of Eisenstein and Gingrich. The computed g's for liquid argon at $T = 126.7°K$ and $n = 1.66 \times 10^{-2}$ particles/Å^3 have also been compared with the Monte-Carlo g of Wood, Parker, and Jacobson. From the computed g's we have calculated energies, pressures, and compressibilities. We have shown that the PY and the CHNC equations can be considered as two different approximations to an exact integral equation. On the basis of this way of looking at the PY and CHNC equations and from the comparison of the computed results we have drawn some conclusions.

I. INTRODUCTION

THE radial distribution function $g(r)$ is defined as the probability of finding two particles at the given relative distance r, averaged over all the possible configurations of the remaining particles in the system. The importance of the radial distribution function in statistical mechanics is due to the fact that all the thermodynamic quantities such as the pressure, internal energy, the free energies, etc. can be calculated from it.[1] The exact expression for the radial distribution function involves integrals of the order of Avogadros number, and therefore the exact values of g cannot be evaluated even with the high-speed computers available. In order to compute g, certain simplifying assumptions are made about the interaction potential between the atoms of the fluid. Besides these assumptions certain mathematical approximations are also necessary so as to reduce the expression for g to a number of integrations which can be performed by a computer.

There are several approaches for the derivation of an integral equation for g. These approaches are very different from one another. All the methods use the same assumptions so far as interatomic potentials are concerned, but the nature of the mathematical approximation is different in each case. We shall discuss only the cluster expansion method.

The cluster expansion method consists of writing the radial distribution function[2,3] as a power series in the density. The coefficients of different powers of the density involve integrals of the order of that power. These coefficients are then expressed as a sum of a product of integrals. These integrals are associated with diagrams obtained by joining two fixed reference points to a

number of field points. These diagrams are classified in accordance with some criteria. (These diagrams have no physical significance.) Finally, a self-consistent integral equation is obtained[4-6] for the radial distribution function. However, this integral equation contains another function which is unknown. In order to obtain an equation which contains only the radial distribution function, the unknown function is expressed in terms of the radial distribution function by neglecting the contribution of a certain class of diagrams. In this way the convolution hypernetted chain (CHNC)[4-6] equation is obtained.

In a similar way, the approximation of the unknown function by the contribution already included in the CHNC approximation and the contribution due to all the other diagrams which will be obtained by joining those diagrams in parallel in all possible ways, results in the Percus-Yevick (PY) integral equation. The Percus-Yervick integral equation was originally derived by them in a very different way.[7] The derivation of the CHNC and PY integral equations on the basis of the cluster expansion of g will be discussed in detail in Sec. II.

The most important assumption involved in the case of potentials is that of additivity of potentials.

The types of approximations and assumptions described above are those which are concerned with the derivation of the integral equations for the radial distribution function. The necessity of these approximations arise because we are dealing with a many-body problem. However, this is not the only many-body problem which occurs when the radial distribution

[1] R. L. Hill, *Statistical Mechanics* (McGraw-Hill Book Company, Inc., New York, 1956).

[2] J. E. Mayer and E. W. Montroll, J. Chem. Phys. **9**, 2 (1941).

[3] E. E. Salpeter, Ann. Phys. (N. Y.) **5**, 183 (1958).

[4] J. M. J. Van Leeuwen, J. Groeneveld, and J. De Boer, Physica **65**, 792 (1959).

[5] E. Meeron, J. Math. Phys. **1**, 192 (1960).

[6] T. Morita and K. Hiroike, Progr. Theoret. Phys. (Kyoto) **23**, 1003 (1960); M. S. Green, technical report, Hughes Aircraft Corp. (unpublished).

[7] J. K. Percus and G. J. Yevick, Phys. Rev. **110**, 1 (1958).

functions are to be derived. One encounters another many-body problem which is that of determining the interatomic potentials between atoms. No satisfactory theoretical treatment of the interatomic potentials exist even in the simplest case of the helium atom. Semi-empirical methods are used to construct interatomic potentials. Unless these potentials are known sufficiently accurately, even an exact integral equation would not yield a radial distribution function which is reliable enough to be used for the determination of the thermo-dynamic properties. It is known that the interatomic potentials consist of a sharp repulsive barrier and an attractive part which goes to zero as r^{-6}. It is expected that at lower temperature the slight differences in the repulsive barrier will not affect the radial distribution function appreciably, while the attractive part of the potential will affect it considerably. At higher tempera-tures, on the other hand, the repulsive part will become more and more important in the determination of the radial distribution function.

The purpose of the present work is twofold. In the first place, we have tried to deduce from theoretical considerations which of the two integral equations would yield better distribution functions under different temperature and density conditions and for different interaction potentials. We have supported our conclu-sions with the help of results of numerical computa-tions whenever they were available. In the second place, we have computed the radial distribution functions of fluid argon at several different values of temperature (all of them are below the critical temperature) and densities. Those values of temperature and density were selected for which x-ray diffraction data were available, and in one case neutron diffraction data were also available. The computed results from the two integral equations are compared with each other, and with the experimental radial distribution functions. The computations have been done using the Lennard-Jones[8] (LJ) 6–12 potential as well as the Guggenheim McGlashan[9] (GM) potential. The GM potential was used because it seems to be more realistic than the LJ potential, and a realistic potential is a necessary re-quirement of the experimental results are to be re-produced from the theoretical computations. From these computations and the theoretical considerations a num-ber of conclusions have been drawn.

In Sec. II we have derived the PY and CHNC in-tegral equations on the basis of the cluster expansion of the radial distribution function and have deduced some conclusions from the theoretical considerations. In Sec. III we have presented the results of computations, comparisons, and conclusions. The two potential func-tions are described in Appendix A.

[8] J. E. Lennard-Jones, Proc. Phys. Soc. (London) **43**, 461 (1931).

[9] E. A. Guggenheim and M. L. McGlashan, Proc. Roy. Soc. (London) **225**, 456 (1960).

II. THE EXACT AND THE APPROXIMATE INTEGRAL EQUATIONS

A. The Exact Integral Equation

In the derivation of the integral equation using the cluster expansion, certain terms are used. The terms are defined below.[10]

(1) Articulation point. This is a point at which cut-ting the diagram will cause it to be separated into two unconnected parts, and one of the two parts will con-tain both reference points. A reference point (reference points are those two points which are not integrated out) can also be an articulation point. See Fig. 1(a).

(2) Irreducible diagram. This is a diagram which does not contain articulation points.

(3) Generic irreducible 1–2 diagram. A diagram con-taining two numbered points, 1 and 2, and k field points which are undistinguishable.

(4) Specific irreducible 1–2 diagram. A diagram containing two numbered reference points, 1 and 2, and k numbered (i.e., distinguishable) points.
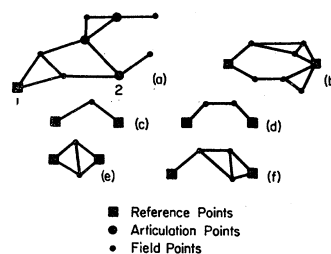

FIG. 1. Reducible dia-gram, (a); irreducible diagrams, (b, c, d, e, f); reference points, articu-lation points, and field points. Simple diagrams, (c, d, e, f); composite diagram, (b).

■ Reference Points
● Articulation Points
• Field Points

(5) Parallel connection of diagrams. When two or more diagrams are connected only at the two reference points, those diagrams are said to be connected in parallel. See Fig. 1(b).

(6) Composite diagram. An irreducible diagram hav-ing at least two parallel connections between 1 and 2. See Fig. 1(b).

(7) Simple diagram. An irreducible diagram having no parallel connection. See Fig. 1(c, d, e, f).

(8) Node. A field point such that every path which connects particles 1 and 2 passes through it.

(9) Nodal diagram. A diagram containing one or more nodes. N is the contribution due to all the nodal diagrams to G.

(10) Elementary diagram. A simple but non-nodal diagram. The direct bond between the reference points is excluded. E is the contribution due to all the elemen-tary diagrams to G.

(11) C set of diagrams contains all the simple and composite diagrams. C is the contribution due to all the simple and composite diagrams to G.

[10] These definitions are the same as used by Leeuwen *et al.* (Ref. 4). Other authors have used some of the terms with slightly different meanings.

(12) S set contains only simple diagrams. S is the contribution due to all the simple diagrams to G.

(13) G set or the extended set contains all the diagrams in the C set together with all the diagrams obtained from the C set by connecting the points 1 and 2 directly and also the diagram containing only the direct bond between 1 and 2.

The quantity $f(r_{ij})$ is defined as

$$f(r_{ij}) = \exp[-\beta\phi(r_{ij})] - 1, \qquad (2.1)$$

where

$$\beta = 1/kT,$$

and ϕ, the interatomic potential

$$\phi(r_{ij}) = \phi(|r_i - r_j|).$$

The pair distribution functions $g(r)$ are related to the pair correlation function G by the equation

$$G(r_{12}) = g(r_{12}) - 1. \qquad (2.2)$$

From the definition of the simple diagrams, nodal diagrams, and the elementary diagrams, we get the relation

$$S(r_{12}) = N(r_{12}) + E(r_{12}). \qquad (2.3)$$

Assuming the validity of classical statistical mechanics and the additivity of potentials, an exact integral equation is derived[11] which is

$$N(r_{12}) = n \int [G(r_{13}) - N(r_{13})] G(r_{23}) dr_3, \qquad (2.4)$$

where[12]

$$G(r_{12}) = \exp[-\beta\phi(r_{12}) + S(r_{12})] - 1. \qquad (2.5)$$

From Eq. (2.3) we see that $N(r)$ is related to $S(r)$ and $E(r)$, and $S(r)$ is related to $G(r)$ and the pair potential $\phi(r)$ through Eq. (2.5). Thus $N(r)$ can be expressed in terms of $G(r)$ and $E(r)$ and we can solve for $G(r)$ from the integral equation (2.4) provided we can find a relation between $E(r)$ and $G(r)$. Since no relation is known between $E(r)$ and $G(r)$, approximations are introduced at this stage.

B. The First Approximation

The first approximation consists of ignoring the contribution due to $E(r)$ (elementary diagrams) in Eq. (2.3) and writing

$$N(r) \approx S(r). \qquad (2.6)$$

This approximation is called the convolution approximation by Meeron[5] and the hypernetted chain approximation by others[4,6] (CHNC). The reasoning behind this approximation may be seen in the following way. If we take any two nodal diagrams and connect them

[11] See Ref. 4, Eq. (28).
[12] See Ref. 4, Eq. (9).

in parallel at the reference points 1 and 2 and then join the two parallel nodal diagrams by at least one bond $f(r_{ij})$, where the ith field point is in the first nodal diagram and the jth field point in the other, we shall get an elementary diagram. If we take three nodal diagrams connected in parallel at the fixed points 1 and 2, then we require at least two bonds $f(r_{ij})$ and $f(r_{kl})$ in order to get an elementary diagram, where the ith field point is in the first nodal diagram, the jth in the second, the kth either in the first or the second, and the lth in the third nodal diagram. In this way any number of nodal diagrams can be linked to one another to give an elementary diagram. If the potential function is such that it falls off very rapidly with distance then the quantity $f(r)$ which is given by Eq. (2.1) will be close to zero for distances greater than r_c where r_c is such that the potential function $\phi(r)$ for $r > r_c$ is practically zero. Thus if such a diagram is to contribute, the ith and jth field points must be at distances smaller than r_c. Hence the integral which contains $f(r_{ij})$ as a factor of its integrand and which is being integrated over r_i and r_j will not contribute much in comparison to the diagrams (which will of course be composite) which do not contain such cross links. The greater the number of such cross links the smaller will become the contribution due to that diagram.

For a repulsive barrier, we can write

$$f(r_{ij}) = \exp[-\beta\phi(r_{ij})] - 1 < 0. \qquad (2.7)$$

For $\phi(r_{ij})$ infinite, $f(r_{ij})$ will equal -1. For an attractive potential, i.e., $\phi(r_{ij}) < 0$, $f(r_{ij}) > 0$.

From Eq. (2.7) we see that an elementary diagram obtained from two or more nodal diagrams connected in parallel and linked together by means of bonds $f(r_{ij})$ as described above will not only decrease in magnitude but also change in sign alternately as links are increased in number one by one. This implies that for short-range repulsive potentials the approximation of neglecting the contribution due to the elementary diagrams will be better than for short-range attractive potentials. Also the approximation $E(r) = 0$ will be better for a potential which increases from zero at $r = r_c$ to higher values as r approaches zero (for example, a potential varying as r^{-n} for $r < r_c$ and zero for $r = r_c$, where n may be any positive number) than for the potential of solid sphere of diameter $r = r_c$.

For repulsive potentials $|f(r_{ij})| < 1$; but for attractive potentials $|f(r_{ij})|$ can be greater than 1 by an amount depending on temperature and the depth of the attractive potential. Hence for attractive potentials this approximation may not be as good as for repulsive potentials.

Now let us consider a potential of the (LJ) type. It contains a sharp repulsive barrier and an attractive part which is deep over a short region and then approaches zero asymptotically from negative values as r^{-6}.

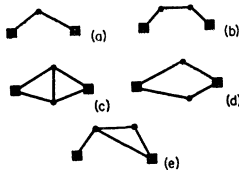Because of the presence of an attractive part, it is

FIG. 2. One and two field points diagrams included in $s(r)$ or $[s(r)]^2$.

clear that the approximation may not be as good as it would be without it.

If kT is very large in comparison to the depth of the attractive part, the quantity $\exp[-\beta\phi(r)]-1$ will be a positive number less than 1 for negative values of $\phi(r)$, and a negative number whose magnitude is less than 1 for positive values of $\phi(r)$. However, the positive values will be much less in magnitude than the negative values. Thus at very high temperatures the effect of the attractive part on g may be washed out. At moderate temperatures the effect of the attractive part will show up because the range of volume over which the attractive part will be effective is usually greater than the volume over which the repulsive part is effective. As the temperature decreases, the contribution of the attractive part on g will go on increasing, and for temperatures equal to or less than the depth of the potential well, the quantity

$$f(r_{ij}) = \exp[-\beta\phi(r_{ij})]-1$$

will be much greater than 1 for values of $\phi(r_{ij})$ in the neighborhood of the bottom of the potential.

Consider a diagram consisting of n nodal diagrams connected in parallel. Connect these nodal diagrams with each other with m links so that the diagram becomes an elementary diagram. This elementary diagram contains m factors $f(r_{ij})$ corresponding to the m bonds. The product of these m factors will sometimes be positive and sometimes be negative depending upon the m different r_{ij}'s. For those links where $\phi(r_{ij})$ is positive, $f(r_{ij})$ will be negative; and for the links for which $\phi(r_{ij})$ is negative, $f(r_{ij})$ will be positive. This means there will be a cancellation when integration is performed over the coordinates of field points which are on the links connecting the parallel nodal diagrams. Hence there is a possibility that the approximation $E(r)=0$ may turn out to be good.

C. The Second Approximation

We set

$$N(r) \approx C(r), \qquad (2.8)$$

where $C(r)$ has been shown[13] to be equal to $e^{S(r)}-1$. Substituting for $N(r)$ in Eq. (2.4), we get

$$e^{S(r_{12})} - 1 = n \int [G(r_{13}) - (e^{S(r_{12})}-1)]G(r_{23})d\mathbf{r}_3.$$

Letting

$$P(r_{12}) = e^{S(12)},$$

we have

$$P(r_{12}) = 1 + n \int [G(r_{13}) - P(r_{13}) + 1]G(r_{23})d\mathbf{r}_3. \quad (2.9)$$

This equation was discovered by Percus and Yevick.[7,14] Now

$$N(r) = S(r) - E(r) = e^{S(r)} - 1 \qquad (2.10)$$

or

$$N(r) = S(r) + \frac{[S(r)]^2}{2!} + \frac{[S(r)]^3}{3!} + \cdots \qquad (2.11)$$

or

$$E(r) = -\left(\frac{[S(r)]^2}{2!} + \frac{[S(r)]^3}{3!} + \cdots \right). \qquad (2.12)$$

The term $[s(r)]^2/2!$ corresponds to the contribution due to all the composite diagrams obtained by joining any two simple diagrams in parallel. The term $[S(r)]^3/3!$ corresponds to the contribution due to all the composite diagrams that will be obtained by joining any three simple diagrams in parallel. Similarly the higher terms give contribution due to composite diagrams obtained by joining several simple diagrams in parallel.

The reason this approximation should be good is not as easy to see as in the previous case. We know that in order to convert a composite diagram into an elementary diagram, the branches of the composite diagrams must be connected by cross links. We also know that the contribution due to each diagram will decrease with the increase in the number of bonds constituting the diagram in the case of repulsive potentials. (We shall discuss the case of attractive potentials later on.) Consider a short-range repulsive potential, as in the previous case, given by r^{-P}, where $P>0$ for $r<r_c$ and zero for $r>r_c$. The smaller the value of P the smaller will be the contribution due to the diagrams with a greater and greater number of bonds in it for a given r_c. This feature is independent of the type of approximations considered.

From Eqs. (2.11) and (2.6) it follows that, if we neglect the higher powers of $S(r)$, then the CHNC and PY approximations become the same. In order to study the PY approximation, we may assume that the third and higher power terms in $S(r)$ in approximation equation (2.12) are negligible in comparison to the $[S(r)]^2$ term. This, however, is not a satisfactory way of looking at the approximation equation (2.12). A better way is to consider the number of field points, the power of density, and the number of crossed links in a diagram. We have already seen that the increase in the number of crossed links reduces the contribution of the diagram. It may be shown[15] that a diagram with k field points is multiplied by a factor n^k, where n is the number density

---

[13] See Ref. 4, Eq. (8a).

[14] J. K. Percus, Phys. Rev. Letters 8, 462 (1962).
[15] See Ref. 4, Eq. (8b).

of particles, in order to form a term of $S(r)$. In the approximation equation (2.11) the terms $S(r)$ and $[S(r)]^2/2!$ are the only terms which contain diagrams with one field point and with two field points. The higher power terms in $S(r)$ contain diagrams with at least three field points. Hence if the density is such that terms involving n^3 or higher powers of n are small compared to n^2, then we can leave the higher powers of $S(r)$ than the second in Eq. (2.11). The terms $S(r)$ and $[S(r)]^2/2!$ also contain terms with more than two field points, but we shall take only those terms which have one or two field points. Figure 2 shows the diagrams which contain one and two field points and are included in $S(r)$ or $[S(r)]^2$. In the PY approximation [considering approximation equation (2.12)] if we consider only the diagram with two field points we get for the contribution due to the elementary diagram

$$E = -\frac{1}{2}\left(n\int f_{13}f_{23}d\mathbf{r}_3\right)^2,$$

while the exact contribution for two field points elementary diagram would be

$$\frac{1}{2}n^2\int\int f_{13}f_{23}f_{14}f_{24}f_{34}d\mathbf{r}_4d\mathbf{r}_3.$$

In effect, for two field points elementary diagrams, we put -1 for f_{34}, the link joining the field points. We can therefore write

$$f_{34} = \exp[-\beta\phi(r_{34})]-1 = -1,$$

which means $\phi(r_{34})$ has been equated to infinity for all values of r_{34}.

Now consider the case of solid spheres. The potential in this case is given by

$$\phi(r) = \infty, \quad r \leq r_c,$$

and

$$\phi(r) = 0, \quad r > r_c.$$

In this case the PY approximation will be good because when points 3 and 4 go farther apart, one or more of the terms f_{13}, f_{14}, f_{23}, f_{24} become zero and thus the error which could have been introduced due to assuming $f(r_{34})$ equal to -1 for all values of r_{34} is small. As is shown in Fig. 3,[16] the approximation of putting $f(r_{34})$ equal to -1 is very good in the case of solid spheres. However, the above considerations are true only up to
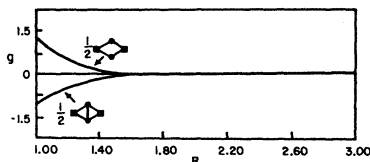
FIG. 4. The three field points elementary (b, c, e, f) and composite (a, d) diagrams.
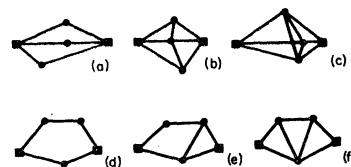
a certain density. If the density is increased we cannot neglect the contribution due to diagrams with more than two field points, and the PY approximation for solid spheres will start to fail. This conclusion is confirmed by the computations of Broyles.[17] This can be seen by examining the three field point diagram included in the $[S(r)]^3/3!$ term shown in Fig. 4(a). There are two elementary diagrams, Fig. 4(b) and Fig. 4(c) from which diagram 4(a) can be obtained. In order to obtain diagram 4(a) from 4(b) we have to remove bonds f_{34} and f_{45}, and in order to obtain 4(a) from 4(c), three bonds, namely, f_{34}, f_{45}, and f_{35}, have to be removed. Now if we let these cross bonds equal -1, then the contribution due to diagram 4(c) will be approximated by the contribution of diagram 4(a) multiplied by -1, which is in accordance with the approximation equation (2.12); but the contribution due to diagram 4(b) should be approximated to the contribution of diagram 4(a) multiplied by $+1$, while the approximation equation (2.12) corresponds to multiplying the contribution of diagram 4(a) by -1, in order to obtain approximately the contribution of the diagram 4(b). This clearly is not correct. Now consider the three field point diagrams included in the $(S)^2$ term. The Fig. 4(d) shows this diagram. The elementary diagram 4(e) and 4(f) can be reduced to 4(d) in the manner described above. The contribution due to 4(e) may be obtained approximately by multiplying by -1, the contribution due to the diagram 4(d). And the contribution due to the diagram 4(b) may be approximated to the contribution of diagram 4(d) multiplied by 1. The latter approximation is not in accord with the approximation equation (2.12). These considerations show that for higher densities the PY approximation may not be good.

The PY approximation, however, will be better for solid spheres than the CHNC approximation which ignores the contribution of elementary diagrams. This conclusion follows from our discussion above, as long as only two field points diagrams are important.

Consider another repulsive potential which varies as r^{-1}, the Coulomb potential. In this case the value of bond $f(r)$ decreases in magnitude continuously with the increase in r but is always negative. In this case also, PY approximation for two field points elementary diagram makes the link between the two field points equal to -1 irrespective of the distance between the field points. However, this approximation might work if we consider that some or all the other bonds, namely, f_{13},

FIG. 3. The contributions due to the elementary and composite diagrams with two field points. (From Klein's thesis.)

[16] M. Klein, thesis, University of Maryland, 1962 (unpublished).

[17] A. A. Broyles, S. U. Chung, and H. L. Sahlin, J. Chem. Phys. 37, 2462 (1962).

TABLE I. Energies, compressibilities, pressures, positions, and heights of first and second maxima and minima in $g(r)$.[a]

T (°K)	$n \times 10^2$	Pt.	Eq.	E'/NkT	Computed $nkTK$	P/nkT	Expt. P/nkT	r_1	$g(r_1)$	r_2	$g(r_2)$	r_3	$g(r_3)$	r_4	$g(r_4)$
		LJ	PY	−8.3386	0.4335	0.45		3.7	3.066	5.0	0.670	7.1	1.253	8.3	0.879
		LJ	CHNC	−8.2462	0.1924	1.12	0.004	3.7	2.902	5.2	0.688	7.1	1.271	8.5	0.889
84.4	2.113	GM	PY	−7.9155	0.6392	0.86		3.6	2.718	4.9	0.644	6.9	1.235	8.2	0.880
		GM	CHNC	−7.7884	−10.8472	−0.83		3.7	2.337	5.1	0.644	7.0	1.167	8.5	0.870
			Neutron diff. expt. at $T=84°$K					3.8	2.45	5.0	0.608				
			x-ray diff. expt.					3.8	3.32						
		LJ	PY	−7.3879	0.3174	1.155		3.7	3.033	5.0	0.661	7.1	1.249	8.3	0.877
91.8	2.059	LJ	CHNC	−7.4626	0.5093	0.272	0.007	3.7	2.749	5.3	0.722	7.1	1.240	8.6	0.908
		GM	PY	−7.1911	1.3286	0.128		3.7	2.541	5.1	0.686	6.9	1.207	8.3	0.905
		GM	CHNC	−6.5569	7.6187	−1.934		3.7	2.003	5.2	0.656	7.2	1.083	8.6	0.904
			x-ray diff. expt.					3.7	2.65	5.3	0.68				
		LJ	PY	−4.2359	0.3838	0.734		3.7	2.472	5.3	0.764	7.1	1.153	8.6	0.941
126.7	1.659	LJ	CHNC	−4.2057	0.5175	0.815		3.7	2.373	5.4	0.792	7.2	1.145	8.8	0.951
		GM	PY	−4.1899	1.1109	0.299	0.064	3.7	2.213	5.4	0.760	7.0	1.140	8.5	0.948
		GM	CHNC	−4.0148	−10.4586	−0.162		3.7	2.000	5.3	0.750	7.1	1.069	8.7	0.916
Monte Carlo		LJ		−3.7794	0.3047	1.1568		3.7	2.220	5.4	0.790	7.4	1.10		
			x-ray diff. expt.					3.66	2.0	5.3	0.75	7.0	1.11		
		LJ	PY	−0.4557	1.8343	0.7608		3.8	2.6679						
		LJ	CHNC	−0.4567	1.8531	0.7609	0.69	3.8	2.6749						
126.7	0.134	GM	PY	−0.5140	2.0221	0.7419		3.8	3.139	6.5	1.1399	6.8	1.1406		
		GM	CHNC	−0.5192	2.0966	0.7413		3.8	3.174	6.4	1.1521	6.9	1.1544		
		LJ	PY	−2.8451	0.7441	0.571		3.7	2.170	5.5	0.860	7.3	1.096	8.8	0.974
		LJ	CHNC	−2.8433	0.7930	0.569	0.146	3.7	2.131	5.6	0.859	7.3	1.092	9.0	0.980
144.1	1.312	GM	PY	−2.9126	1.4081	0.322		3.7	2.089	5.3	0.829	7.1	1.110	8.7	0.970
		GM	CHNC	−2.9465	1.7119	0.247		3.7	2.075	5.4	0.843	7.1	1.118	8.8	0.975
			x-ray diff. expt.					3.69	2.035	5.82	7.18	1.1	1.1		
144.1	0.333	LJ	PY	−0.9136	3.2294	0.5727	0.533	3.8	2.377						
		LJ	CHNC	−0.9261	3.5446	0.5729		3.8	2.416						
		LJ	PY	−2.3506	1.0540	0.462		3.7	2.081	5.6	0.883	7.3	1.079	9.0	0.988
149.3	1.112	LJ	CHNC	−2.3581	1.1728	0.450		3.7	2.060	5.7	0.895	7.4	1.079	9.2	0.991
		GM	PY	−2.4470	1.9156	0.309	0.207	3.7	2.088	5.4	0.872	7.1	1.106	8.8	0.987
Case I		GM	CHNC	−2.4822	2.2698	0.267		3.7	2.094	5.4	0.886	7.2	1.118	8.9	0.991
Case II		GM	CHNC	−2.1906	−6.6449	0.072		3.8	1.765	5.4	0.795	7.3	0.960	8.9	0.904
			x-ray diff. expt.					4.01	1.489	5.64	0.78	7.25	1.11		
		LJ	PY	−1.2531	4.0002	0.465		3.8	2.265	6.1	1.064	7.4	1.132		
149.3	0.498	LJ	CHNC	−1.2770	4.6514	0.468	0.433	3.8	2.316	6.1	1.081	7.4	1.157		
		GM	CHNC	−0.8908	−7.6808	0.532		3.8	1.583	5.9	0.726	8.1	0.774		
			x-ray diff. expt.					3.8	1.94						

[a] T is the temperature in degrees Kelvin, n is the number of particles per cubic angstrom, Pt. =potential, Eq. =equation, r_1 is the position of the first maximum in g, r_2 is the position of the first minimum in g, r_3 is the position of the second maximum in g, r_4 is the position of the second minimum in g, Diff. =diffraction.
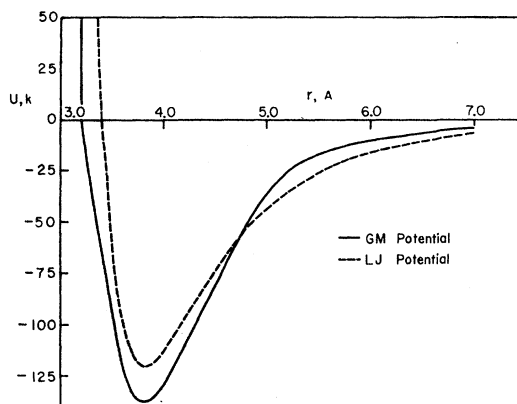

FIG. 5. The Lennard-Jones and Guggenheim-McGlashan potentials. The distance is in angstroms and the energy in degrees Kelvin.

f_{14}, f_{23}, and f_{24} decrease in magnitude as the distance between the points which they join increases. The PY approximation will give lower values of g than the actual value because the bonds f_{13}, f_{14}, f_{23}, and f_{24} do not decrease sufficiently rapidly; the CHNC approximation will give higher values because f_{34} in this approximation is being equated to zero for all values of r_{34}. The actual value of g for the Coulomb case will be bracketed by the CHNC g and the PY g. These considerations are valid as long as the contributions to g due to three or more field points diagrams are negligible.

Now we shall discuss the case where the potential between the particles has an attractive part also, i.e., a potential of the Lennard-Jones type.

When the temperature (in energy units) is high in comparison to the depth of the potential at the minimum then we can treat the LJ potential for the present
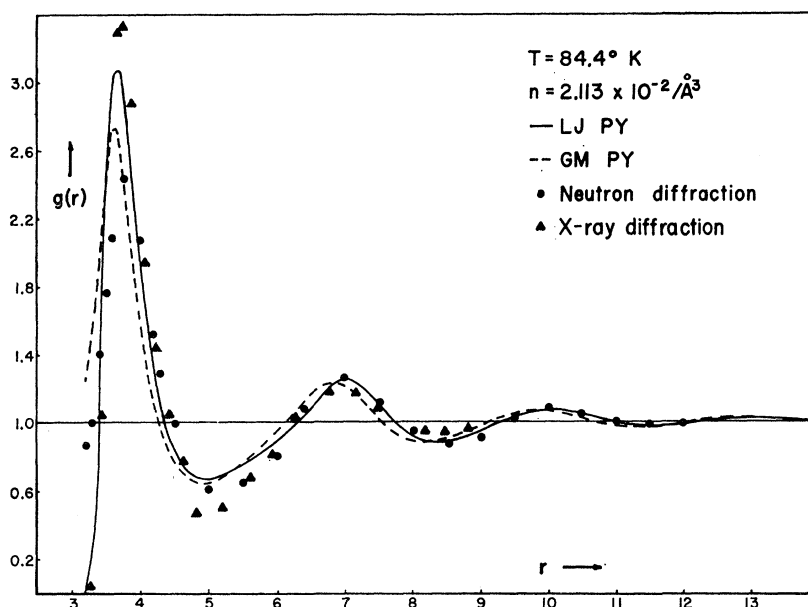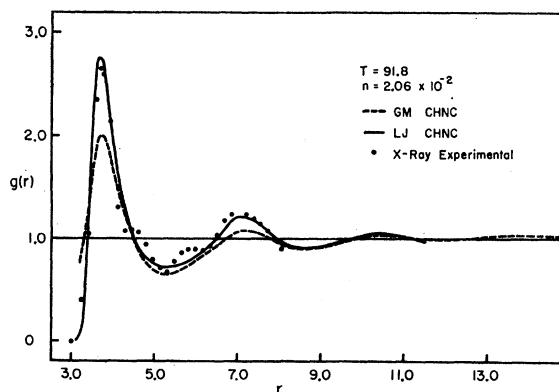
FIG. 6. The computed g's from the CHNC equation with the GM and LJ potentials at 84.4°K. The x-ray diffraction points are due to Eisenstein and Gingrich. The neutron diffraction points are due to Henshaw.
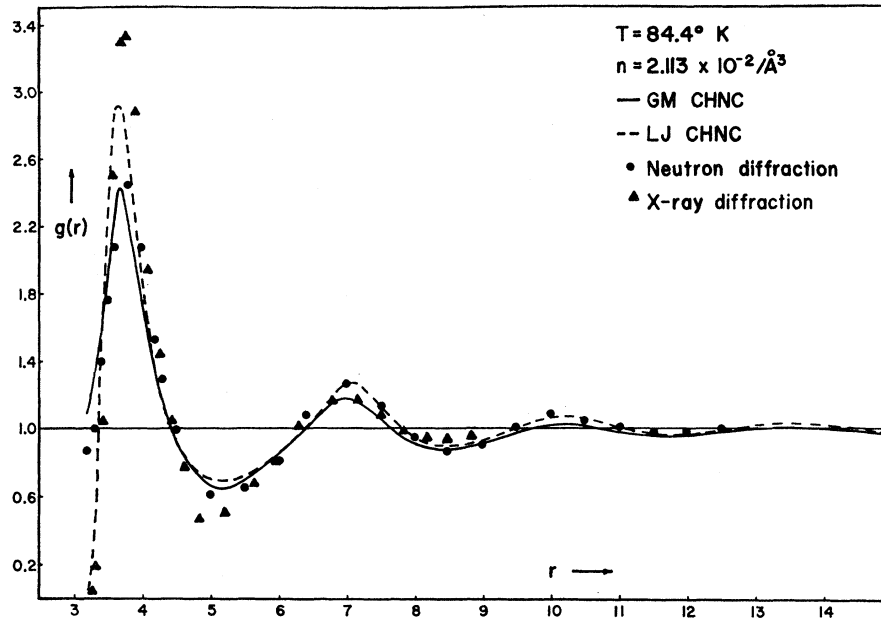
consideration close to the case of solid spheres. As the temperature decreases the attractive part of the potential becomes more and more effective. If the density of the particles is so low that we need not consider the elementary diagrams with two field points, the PY and the CHNC approximations should give the same results. At low temperatures with low densities the small changes in the potential must make the difference in the computed distribution functions and would be a good way to separate the inaccuracies in the integral equations from the inaccuracies in the interatomic potentials, particularly in the attractive part of the potential.

But, when the density is so high that the two field points elementary diagrams must be taken into consideration; the PY approximation and the CHNC approximation must give different results. The PY approximation assumes $f(r_{34})$ to be -1 for all values of r_{34}; but in this case, as we have seen in the discussion of CHNC approximation, $f(r_{34})$ can take positive values, and also much greater than 1, depending on the temperature and the value of the minimum in the potential. Recalling the discussion in the case of CHNC approximation, we conclude that the PY approximation cannot be expected to be good for this case.

III. RESULTS OF COMPUTATIONS, COMPARISONS, AND CONCLUSIONS

A. Results of Computations

Radial distribution functions g for argon fluid have been computed from the Percus-Yevick and the convolution hypernetted chain equations, at various temperatures and densities. The method of computation

is described in Refs. 17 and 18. All the temperatures at which the computations have been done are below the critical temperature ($T_c = 150.66°K$). We have used two different interaction potentials, (i) the Lennard-Jones 6–12 potential and (ii) the Guggenheim-McGlashan potential. (See Appendix A.) The computed g's are plotted in Figs. 6–18, and are given in tabular form in Ref. 18.

From the g's we have computed the quantity J, which is the coherent scattering per particle[19] I_{eu}/N. (I_{eu} is the total scattering in electron units and N is the total number of scattering particles.)

$$J = [1+i(s)]f^2, \qquad (3.1)$$

where $i(s)$ is given by equation[19]

$$si(s) = 4\pi n \int_0^\infty r[g(r)-1] \sin(sr)dr, \qquad (3.2)$$

f is the atomic structure factor and n is the macroscopic density of particles. The computed J's are plotted in Figs. 19 to 31, and are given in tabular form in Ref. 18.

From the g's we have computed the quantities E'/NkT, $nkTK$, and P/nkT, where E' is the internal energy, K is the isothermal compressibility, and P is the pressure. The quantity E' is given by the equation[1]

$$E'/NkT = (2\pi n/kT) \int_0^\infty \phi g r^2 dr. \qquad (3.3)$$

---

[18] A. A. Khan, Ph.D. thesis, University of Florida, 1963 (unpublished).

[19] N. S. Gingrich, Rev. Mod. Phys. **15**, 90 (1943).

FIG. 7. The computed g's from the PY equation with the GM and LJ potentials at 84.4°K. The x-ray diffraction points are due to Eisenstein and Gingrich. The neutron diffraction points are due to Henshaw.

The quantity K is given by the equation[20]

$$nkTK = 1 - 4\pi n \int_0^\infty (1-g)r^2 dr, \qquad (3.4)$$

and the quantity P is given by[1]

$$P/nkT = 1 - (2\pi n/3kT) \int_0^\infty \phi' g r^3 dr, \qquad (3.5)$$

where N is the total number of particles in the system, n is the number of particles per unit volume, and ϕ is the interatomic potential. Results of computations of energy, pressure, and compressibility are given in Table I.
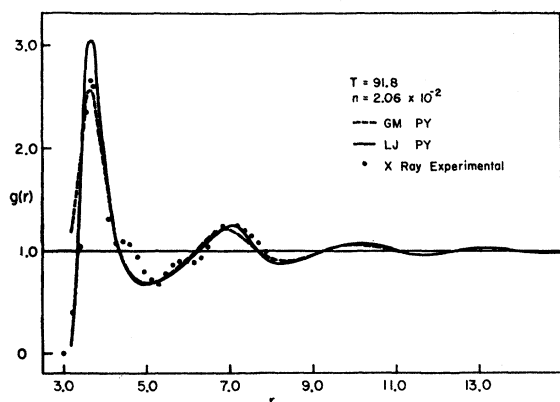

FIG. 8. The computed g's from the CHNC equation with the GM and LJ potentials at 91.8°K. The x-ray diffraction points are due to Eisenstein and Gingrich.

[20] L. D. Landau and E. M. Lifshitz, *Statistical Physics* (Addison-Wesley Publishing Company, Inc., 1958).

B. Comparison of the g's

For a given density and temperature the following comparisons of g's have been made:

(i) g's computed from the same integral equation but with the two different potentials (LJ and GM potentials).

(ii) g's computed from the same potential but with the different integral equations (PY and CHNC integral equations).

(iii) All the computed g's with the experimental g's. We have used x-ray experimental[21] radial distribution functions of Eisenstein and Gingrich.[22] The computed distribution functions for the case of $T=84.4$°K have also been compared with the g obtained experimentally from neutron diffraction experiments by Henshaw[23] in liquid argon at 84°K.

In order to compare the distribution functions obtained with the same integral equation and with different potentials, we have plotted the g's computed by using the LJ and GM potentials on the same graph. Experimental curves have also been plotted on these graphs (see Figs. 6–18). Figure 5 shows how the two potentials look compared to each other. Since the GM potential has a vertical barrier, the g's computed from this potential are zero for values less than 3.2 Å. Also, the effect of the vertical barrier is to give higher values of g for values of r close to 3.2 Å. This effect can be seen in all the cases. This effect of higher values of g's seems to extend farther and farther away from 3.2 Å as the

[21] Experimental values of g were read from the photographically enlarged curves of the published curves.

[22] A. Eisenstein and N. S. Gingrich, Phys. Rev. **62**, 261 (1942).

[23] D. G. Henshaw, Phys. Rev. **105**, 976 (1957).

temperature is increased and the density is decreased. Keeping the temperature (126.7°K) the same and changing the density so that we pass from the liquid to the vapor state, the GM potential gives higher values for g than the LJ potential almost everywhere. The first peak for GM potential is considerably higher than for the LJ potential. However, these high values of g for GM potential at the first peak and beyond the first peak do not depend on the fact that the GM potential has a vertical barrier (see Figs. 11–13.)

The height of the first peak in the g is higher for the LJ potential than for the GM potential for temperatures 84.4, 91.8, 126.7, and 144.1°K in the liquid state. (See Table I and Figs. 6–9, 11, 14, and 15.) The height of the first peak is lower for LJ potential than for the GM potential for the cases of $T=149.3°K$, $n=1.112 \times 10^{-2}$ particles/Å³ (we are not considering GM, CHNC, case II) which is the lowest density in the liquid state that we have studied, and for the $T=126.7°K$, $n=0.134\times10^{-2}$ particles/Å³, which is a vapor state. We have not been able to obtain solutions for the integral equations with the GM potential in the vapor state of argon at 144.1°K, and for argon vapor at 149.3°K for the GM potential and the PY equation. We obtained a solution for argon vapor at 149.3°K for the GM potential and CHNC equation, but probably this solution corresponds to the case II GM, CHNC, g for liquid argon at 149.3°K which we consider to be an invalid solution. We can conclude that the first peak for the GM potential is lower than that for the LJ potential for densities equal to or higher than 1.312×10^{-2} particles/Å³ for the range of temperatures we have studied. This effect is rather unexpected in view of the fact that the GM potential is deeper and has a greater bowl width.

The first peak for liquid densities for both the potentials occur at 3.7 Å with one exception ($T=84.4$, GM, PY peak is at 3.6 Å). For densities in the vapor region, the first peak appears at 3.8 Å for both the
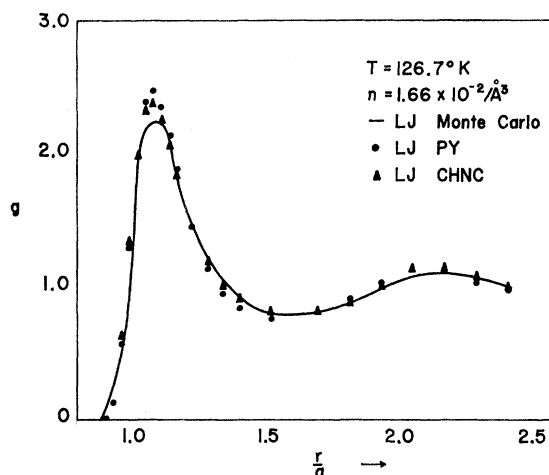
FIG. 10. The computed g's from the PY and CHNC equations with the LJ potential at 126.7°K. The Monte-Carlo g is due to Wood, Parker, and Jacobson.

potentials. In Table I are given the positions and heights of the first and second maxima and minima for the purpose of comparison.

Comparison of internal energies show that the energies computed from the LJ potential are less than those computed from GM potential for both the integral equations, for liquid argon for densities higher than 1.6×10^{-2} particles/Å³, in the temperature range studied. For lower liquid densities and for vapors the energies are lower for the case of the GM potential.

Comparison of compressibilities show that the PY equation with the LJ potential gives lower values than those computed from the GM potential and PY equation in all the cases studied. For the CHNC equation with the GM potential we obtained negative values for compressibilities for $T=84.4°K$ case and $T=126.7°K$, $n=1.66\times10^{-2}$ particles/Å³ case. In all other cases the compressibilities calculated from the CHNC equation with the LJ potential are less than those given by the CHNC equation with GM potential.

In all the cases studied the pressures computed from the LJ potential are higher than those calculated from the GM potential for both the integral equations except for the case $T=84.4°K$ in which the LJ potential with the PY integral equation gives a lower value than the GM potential with the PY equation.

The values of compressibilities and pressure computed using the LJ potential are very much different from those computed using the GM potential at liquid argon densities. The difference in the internal energies is small. (See Table I.) From this we see that at temperatures below the critical temperature and at liquid densities the thermodynamic quantities like pressure and isothermal compressibility are extremely sensitive to the interaction potential.

To compare the integral equations, it would be best to know the exact g for a given type of interaction.
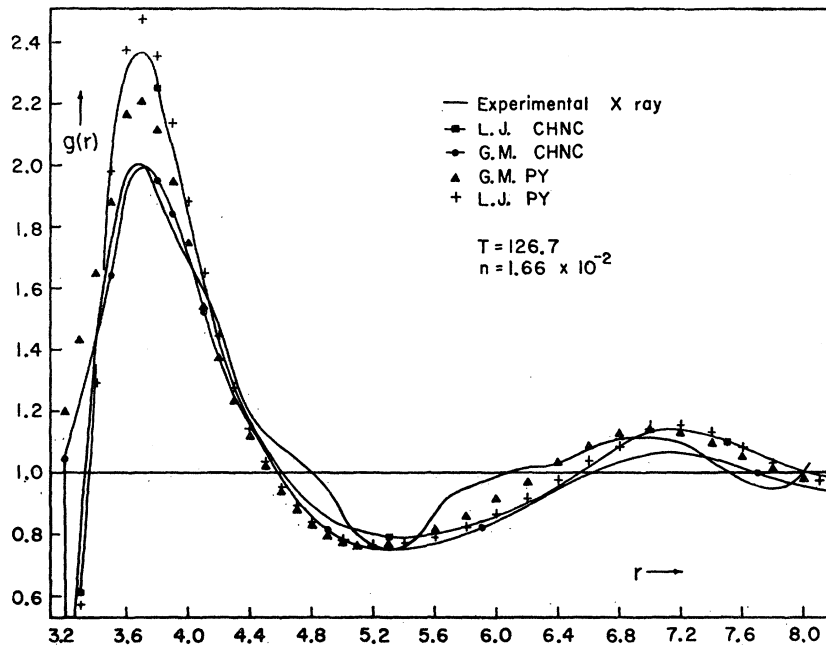

FIG. 9. The computed g's from the PY equation with the GM and LJ potentials at 91.8°K. The x-ray diffraction points are due to Eisenstein and Gingrich.

Fortunately, we have the Monte Carlo g computed by Wood, Parker, and Jacobson[24] for the LJ potential, at $T = 126.7°K$. Computations at this temperature and density ($n = 1.66 \times 10^{-2}$ particles/Å³) were done by Verlet and Levesque[25] with the PY and CHNC integral equations using the LJ potential. Our computations agree with theirs. In Fig. 10 we have plotted the g's computed from the PY and CHNC integral equations for this case. The continuous curve is the Monte Carlo curve. The abscissa is in units of a ($a = 3.405$ Å). It can be seen that the Monte Carlo curve and PY points everywhere bracket the CHNC points. The agreement between the Monte Carlo curve and the CHNC points

is good except at the first peak. The improved agreement of the CHNC relative to the PY solution when compared to Monte Carlo is to be expected at this lower temperature from the considerations in Sec. II. We computed from the Monte Carlo g (Monte Carlo g is given up to 8.4 Å) the energy E', the compressibility[26] K, and the pressure P. The computed E' and P from the PY and CHNC equation are close but the K's in the two cases are very different. The agreement with the Monte Carlo values is not good. (See Table I.) This shows how sensitive the thermodynamic quantities are to small differences in the g's, since Fig. 10 shows rather good agreement among the three distribution functions.
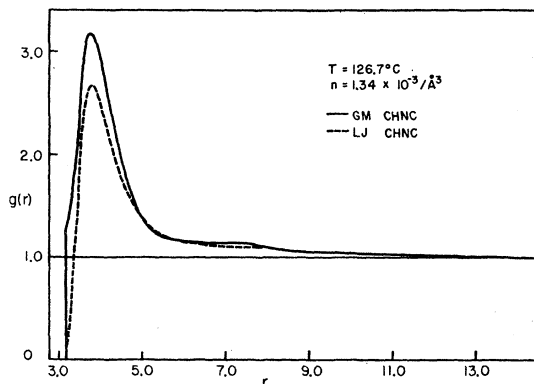
Fig. 12. The computed g's from the CHNC equation with the GM and LJ potentials for argon vapor at 126.7°K.
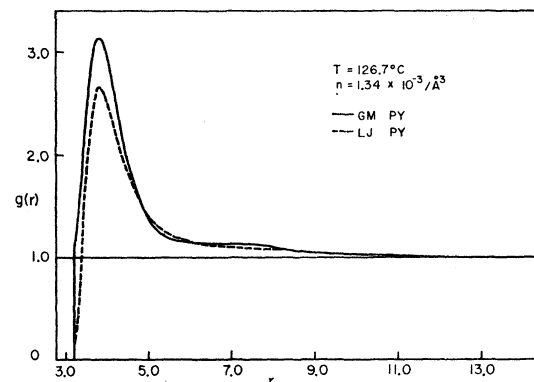
Fig. 13. The computed g's from the PY equation with the GM and LJ potentials for argon vapor at 126.7°K.

[24] W. W. Wood, F. R. Parker, and J. D. Jacobson, Nuovo Cimento Suppl. 9, 133 (1958).

[25] L. Verlet and D. Levesque, Physica 28, 1124 (1962).

[26] The Monte Carlo K is not likely to be good because of the strong dependence of K on g at large r.
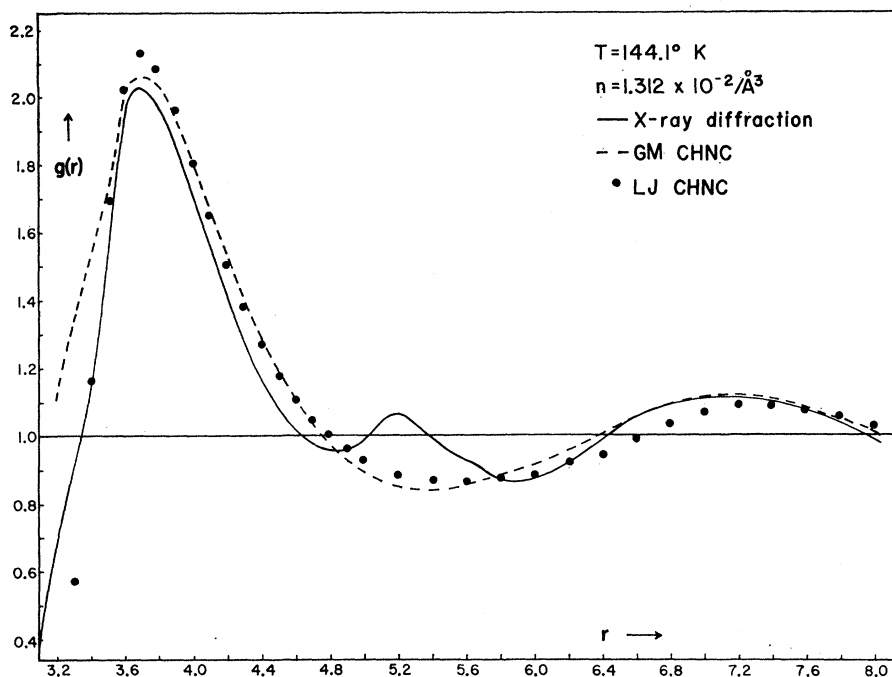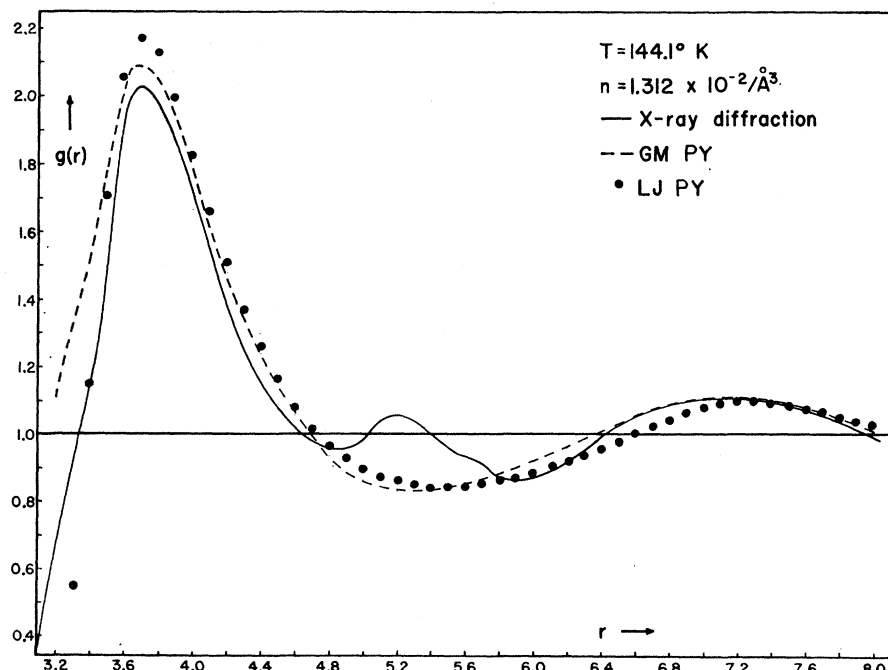
FIG. 14. The computed g's from the CHNC equation with the GM and LJ potentials at 144.1°K. The x-ray diffraction curve is due to Eisenstein and Gingrich.

Since the experimental distribution function is also available for this case, we compared g's from the two integral equations using the LJ and GM potentials with the experimental g. Since the Monte Carlo calculations have been done with the LJ potential, the difference between the experimental g and the Monte Carlo[24] g is due to the fact that the LJ potential is not a realistic potential (see Fig. 11).

In order to see how good the GM potential is in comparison to the LJ potential, first we studied a case of low density (vapor state) at low temperature. We saw in Sec. II that as long as the density is so low that the diagrams with more than one field point do not contribute appreciably, the CHNC and PY equations must give almost the same g for a given potential of interaction. We have computed g's from the PY and the

FIG. 15. The computed g's from the PY equation with the GM and PY equation at 144.1°K. The x-ray diffraction curve is due to Eisenstein and Gingrich.
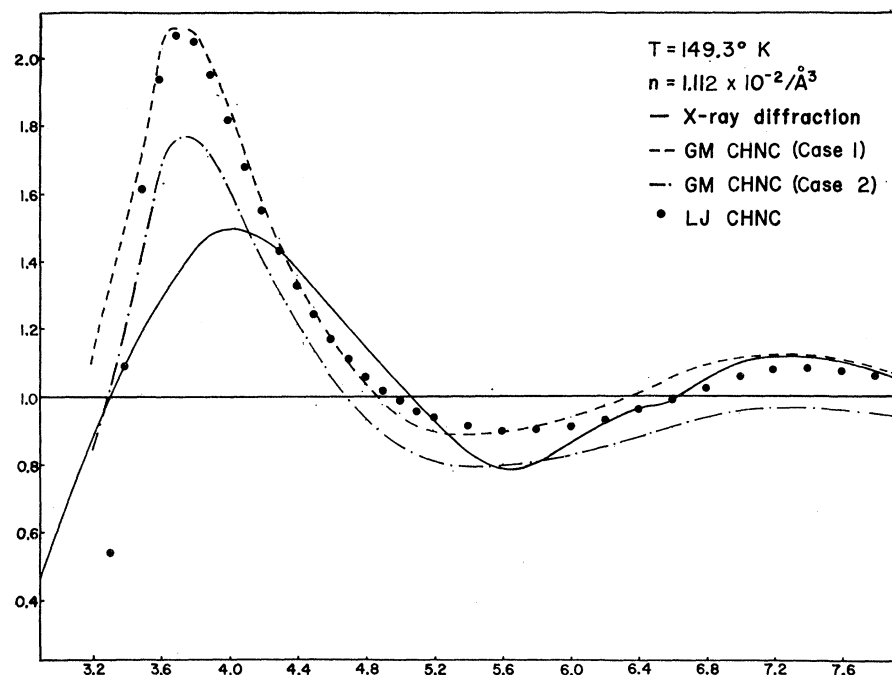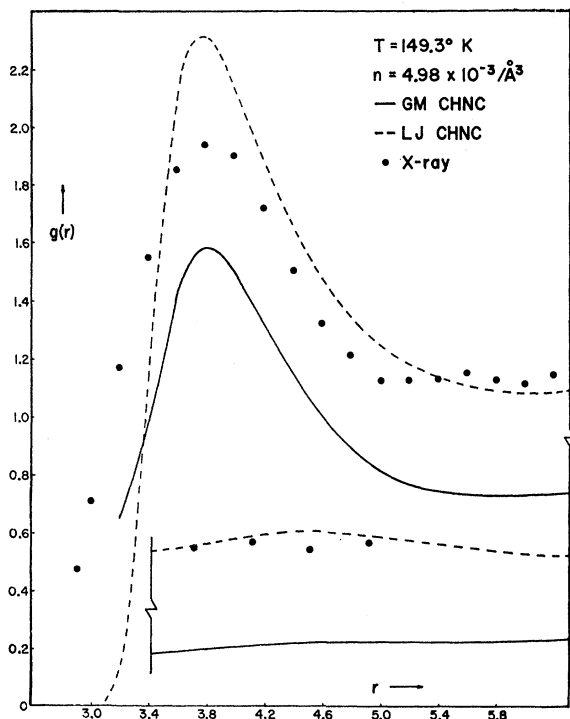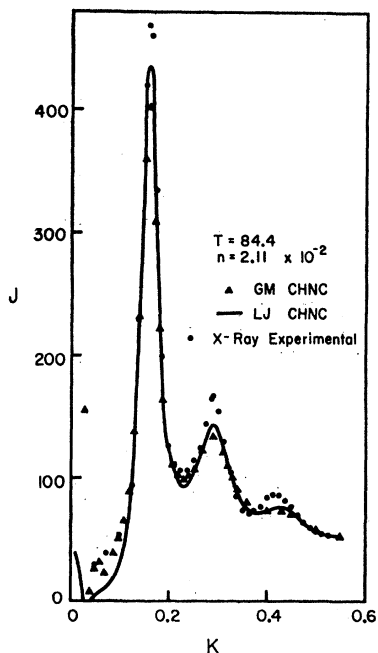
FIG. 16. The computed g's from the CHNC equation with the GM and LJ potentials at 149.3°K. Case 1 and case 2 correspond to two different solutions obtained with the GM potential. The x-ray diffraction curve is due to Eisenstein and Gingrich.

CHNC integral equations using the LJ and GM potentials, at $T=126.7$°K and $n=1.34\times10^{-3}$ particles/Å³ (vapor state). From the Figs. 12 and 13, it will be seen that there is little difference in the g's computed from the different integral equations, but there is a sharp difference when the potential function is changed. From these g's we have computed the pressures, and compared them with the experimental value. (See Table I.) The LJ potential with the CHNC or the PY equation gives the pressure $(P/nkT)0.76$ and the GM with the CHNC or with the PY gives the pressure 0.74, while the experimental value is 0.69. This comparison shows that the GM potential is more realistic. (This conclusion is valid as long as the temperatures are low
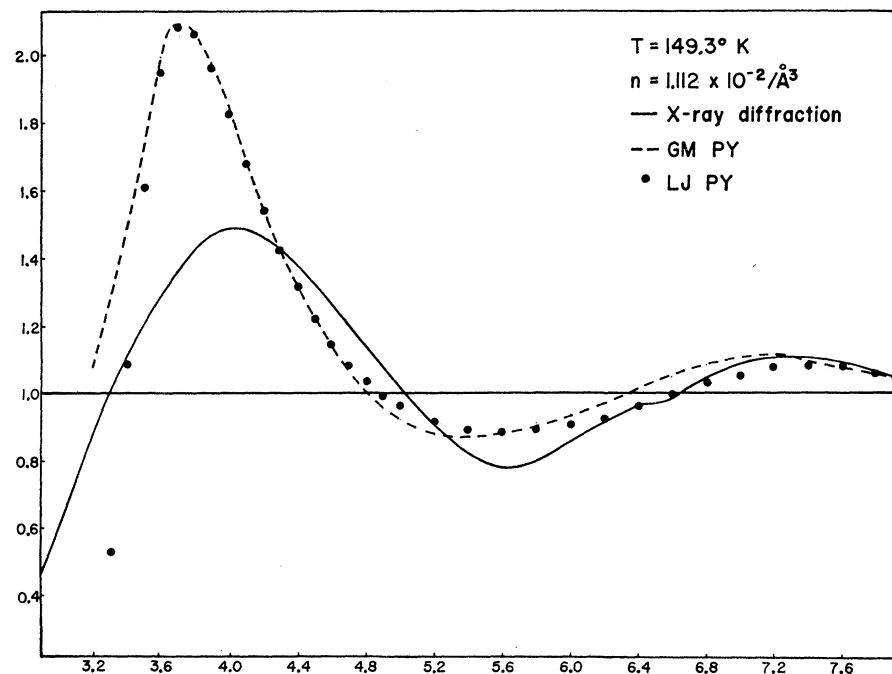
FIG. 17. The computed g's from the PY equation with the GM and LJ potentials at 149.3°K. The x-ray diffraction curve is due to Eisenstein and Gingrich.

FIG. 18. The computed g's from the CHNC equation with the GM and LJ potential for argon vapor at 149.3°K. The x-ray diffraction points are due to Eisenstein and Gingrich.

enough that the attractive part of the potential is more important.)

In Fig. 11 we have plotted the x-ray experimental g,[22]

FIG. 19. The computed J's from the CHNC equation with the GM and LJ potentials at 84.4°K. The x-ray diffraction points are due to Eisenstein and Gingrich.
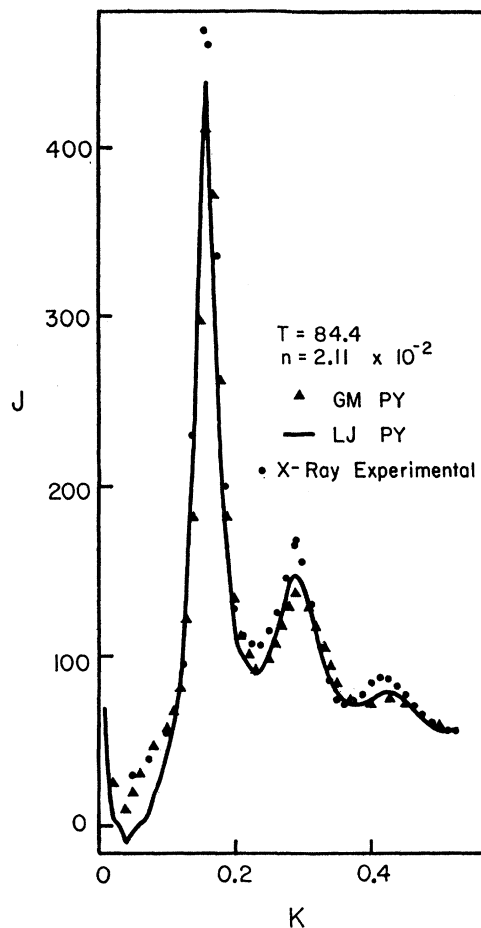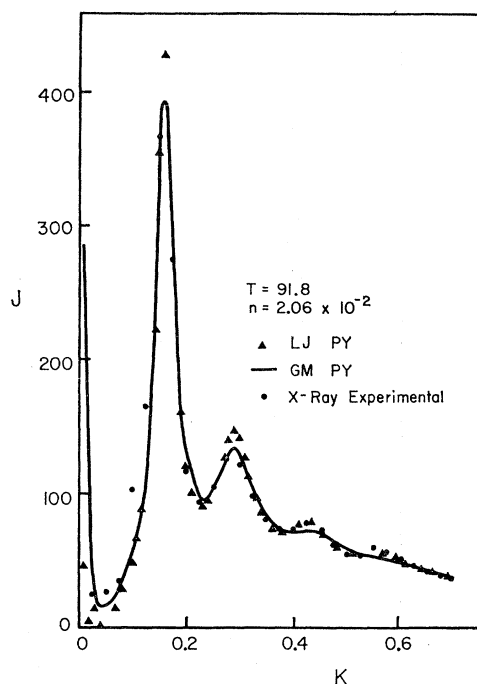

FIG. 20. The compound J's from the PY equation with the GM and LJ potentials at 84.4°K. The x-ray diffraction points are due to Eisenstein and Gingrich.

and the computed g's from the two integral equations using the LJ and GM potentials at $T=126.7$ and $n=1.66\times10^{-2}$ particles/$Å^3$. The agreement with the experimental curve is best for the case of the GM potential with the CHNC equation. It is interesting to note that it is the CHNC equation which gives better agreement with the Monte Carlo g;[24] and it is the pressure computed from the g obtained from any of the two integral equations using the GM potential that gives better agreement with the experimental pressure in the case of argon vapor at 126.7°K discussed above. Hence, it follows that, for the liquid argon case at 126.7°K, the CHNC equation is doing a better job than the PY equation. However, if the GM potential and the x-ray g had been accurate enough we should have gotten the peak of the g, in the case of liquid argon at 126.7°K computed from GM potential and CHNC equation, a little higher than the peak of the experimental g. This is because the peak in the CHNC g is a little higher than the peak of the Monte Carlo g (see Fig. 10). Hence, if the peak in the x-ray experimental g is taken as correct,

FIG. 21. The computed J's from the CHNC equation with the GM and LJ potentials at 91.8°K. The x-ray diffraction points are due to Eisenstein and Gingrich.

the GM potential must not be good enough (although better than LJ potential) for the computation of radial distribution functions which will give reliable thermodynamic quantities. Even in the case we have discussed above, the computed pressure does not agree with the experimental pressure at all. The computed pressure is a negative quantity (-0.162). If we consider the magnitude, then it is closer than any other computed pressure to the experimental pressure (see Table I).

In all the liquid argon cases studied, the PY equation gives a higher first peak in the computed g's using either of the potentials, except in the case of $T=149.3°K$. In this case, using the GM potential and the PY equation, the first peak in the g is 2.088 while with the CHNC equation case I, the first peak is 2.094. In argon vapor, the g's computed from the CHNC equation have higher first peaks than those computed from the PY equation (see Table I).

At temperatures lower than 126°K the difference in the first peak of g computed from the PY and CHNC equations is greater for the GM potential. This is due to the greater depth bowl and bowl width of the GM potential which becomes more effective at lower temperatures (see Table I).

The PY and CHNC equations give energies which are very close for a given potential. The change in potential causes considerable change in the internal energies (see Table I).

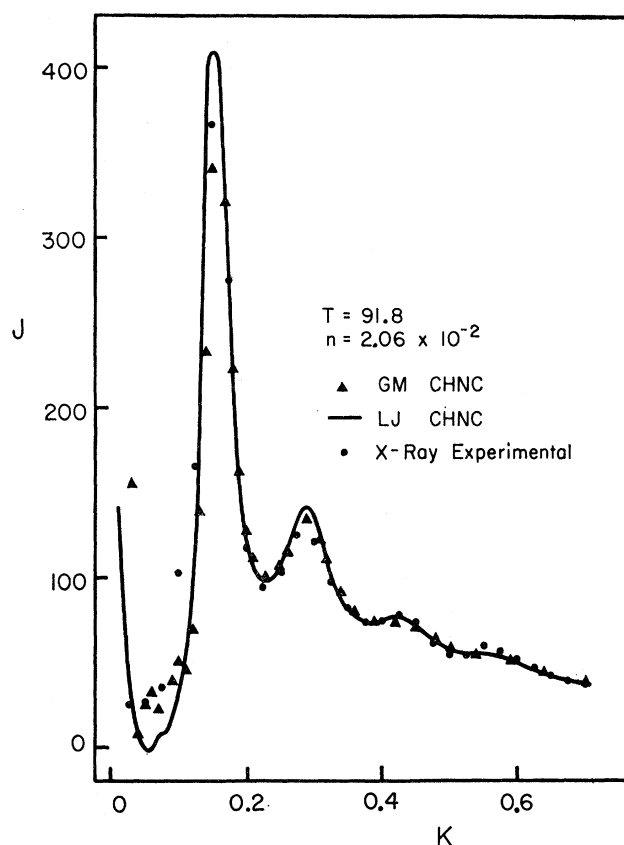The compressibilities computed from the CHNC and the PY equations for the same potential are very dif-

FIG. 22. The computed J's from the PY equation with the GM and LJ potentials at 92.8°K. The x-ray diffraction points are due to Eisenstein and Gingrich.

ferent at temperatures 84.4, 91.8 and 126.7°K for liquid argon. For lower densities and for higher temperatures they are close (see Table I).
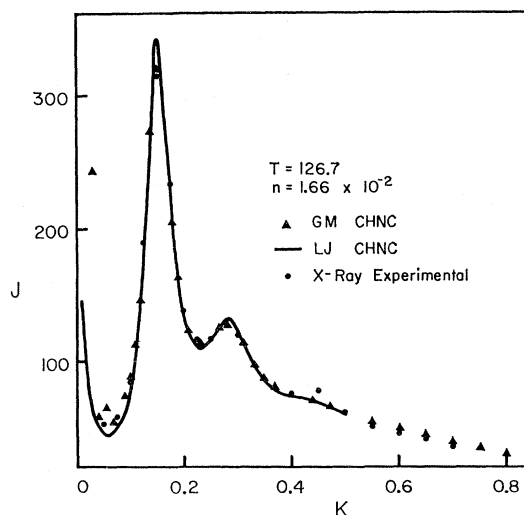

FIG. 23. The computed J's from the CHNC equation with the GM and LJ potentials at 126.7°K. The x-ray diffraction points are due to Eisenstein and Gingrich.

The computed pressures from the two integral equations are also not in agreement for lower temperatures (84.4, 91.8°K) for liquid argon. For 126.7°K (liquid argon) the agreement is better for the LJ potential but there is considerable difference for the GM potential. The GM potential with the CHNC equation gives a negative value of pressure. In all other cases the values
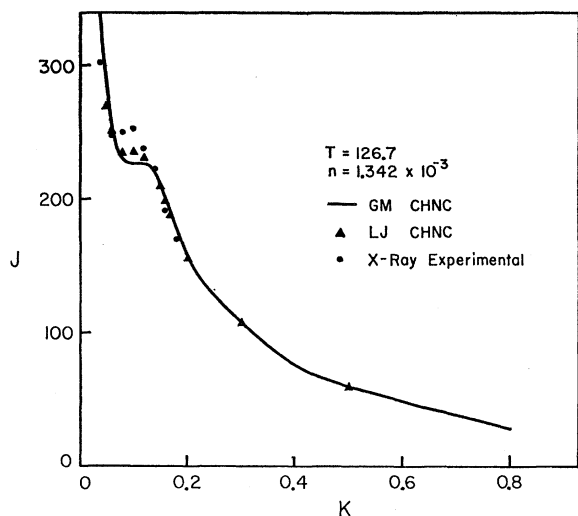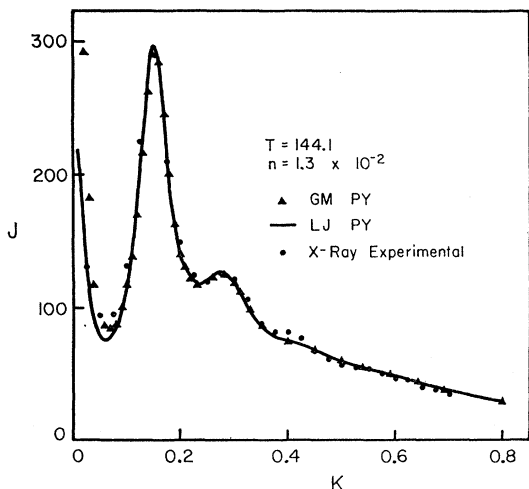

FIG. 24. The computed J's from the CHNC equation with the GM and LJ potentials for argon vapor at 126.7°K. The x-ray diffraction points are due to Eisenstein and Gingrich.

of pressure computed from the CHNC and PY equation agree quite well for the LJ potential but the differences is considerable for GM potential.

The experimental[22,23] distribution functions have been plotted on Figs. 6–9, 11, and 14–18. In the case of liquid argon at 126.7°K, the expermental, curve is closest to

FIG. 25. The computed J's from the CHNC equation with the GM and LJ potentials at 144.1°K. The x-ray diffraction points are due to Eisenstein and Gingrich.
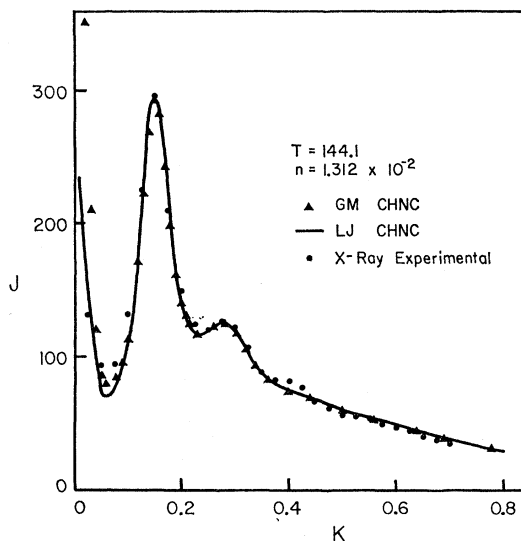

FIG. 26. The computed J's from the PY equation with the GM and LJ potentials at 144.1°K. The x-ray diffraction points are due to Eisenstein and Gingrich.

to the curve computed with the CHNC equation for the GM potential (see Fig. 11). In the case of 144.1°K, $n = 1.312 \times 10^{-2}$ particles/Å³, all the computed curves seem to be equally good compared to the experimental
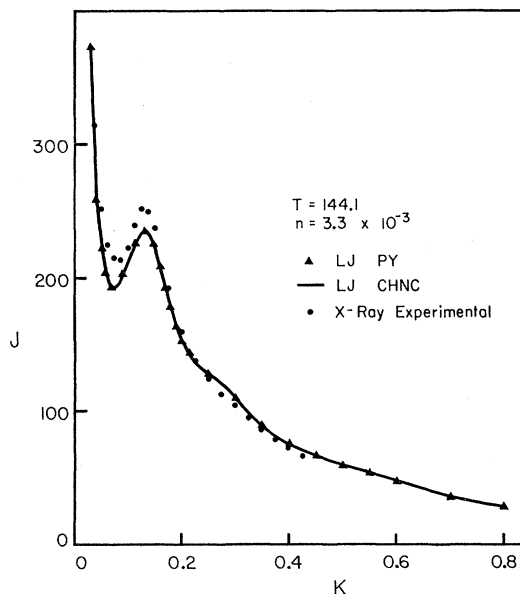

FIG. 27. The computed J's from the PY and CHNC equation with the LJ potential for argon vapor at 144.1°K. The x-ray diffraction points are due to Eisenstein and Gingrich.

curve. However, if we take into consideration the height of the first peak, the best is again the CHNC equation with the GM potential. The experimental curve is very much different from the computed curves in the cases of $T = 149.3$°K, $n = 1.116 \times 10^{-2}$ particles/Å³ and for
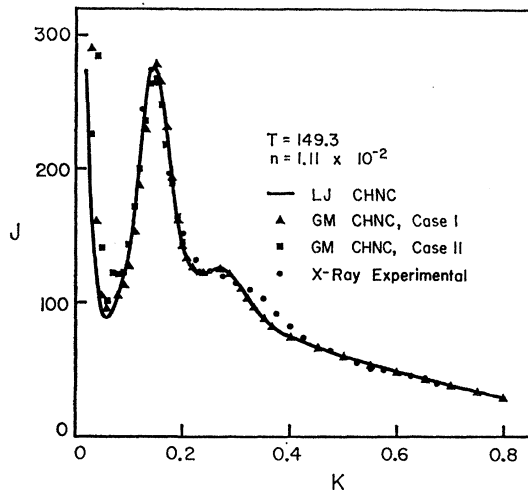
FIG. 28. The computed J's from the CHNC equation with the GM and LJ potentials at 169.3°K. The Case I and case II refer to the two solutions obtained with the GM potential. The x-ray diffraction points are due to Eisenstein and Gingrich.

$T=149.3°K$ and $n=4.98\times10^{-3}$ particles/Å³. In the case of $T=84.4°K$, the agreement between the computed g with the GM potential and CHNC equation and the neutron diffraction curve is quite good. On the other hand, none of the computed curves are in agreement with the x-ray experimental distribution function. Verlet and Levesque[25] compared the neutron diffraction
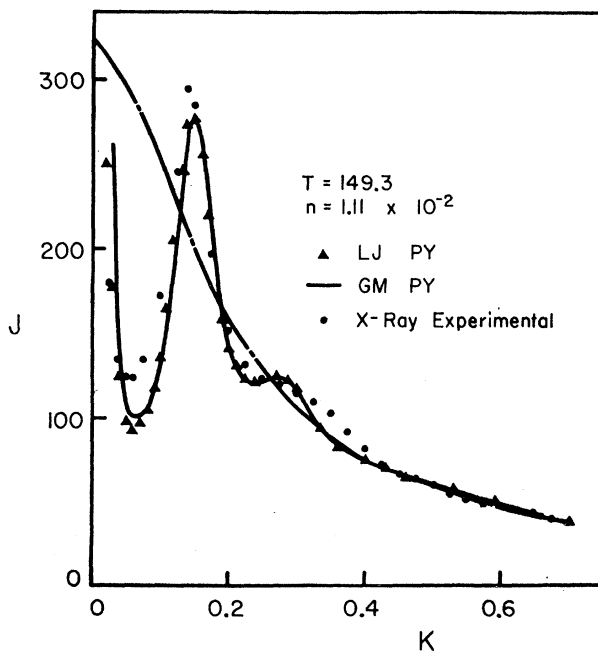

FIG. 29. The computed J's from the PY equation with the GM and LJ potentials at 149.3°K. The x-ray diffraction points are due to Eisenstein and Gingrich. The f^2 (f is atomic structure factor) curve is also plotted.

intensity curves with the computed intensity curves for the LJ potential and CHNC equation and qualitatively the agreement was good, but there was considerable difference at the first peak. With the GM potential the fit at the first peak (in the radial distribution function curve) is much better (see Fig. 6).

A comparison of the computed pressure with the experimental pressure shows that the agreement is, in general, very bad (see Table I). However, in general at
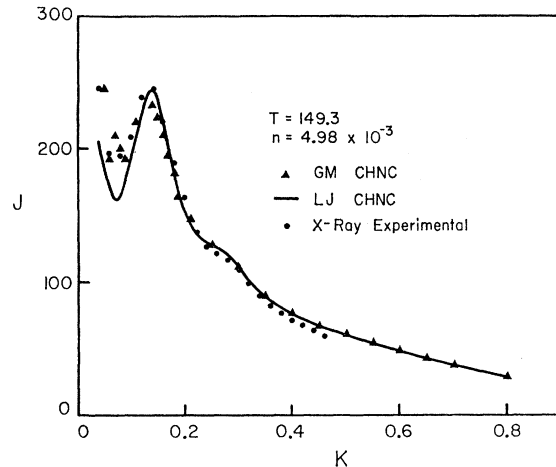

FIG. 30. The computed J's from the CHNC equation with the GM and LJ potentials for argon vapor at 149.3°K. The x-ray diffraction points are due to Eisenstein and Gingrich.

higher temperatures and lower densities studied, the CHNC equation with the GM potential gives pressures which are nearer to the experimental pressure than the other computed pressures.

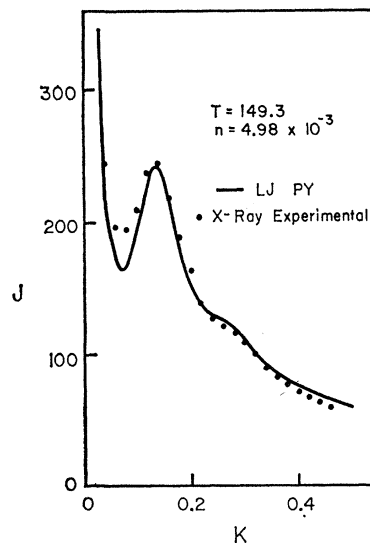In the case of $T=149.3°K$ and $n=1.112\times10^{-2}$ particles/Å³ with the GM potential and CHNC equa-

FIG. 31. The computed J's from the PY equation with the LJ potential for argon vapor at 149.3°K. The x-ray diffraction points are due to Eisenstein and Gingrich.
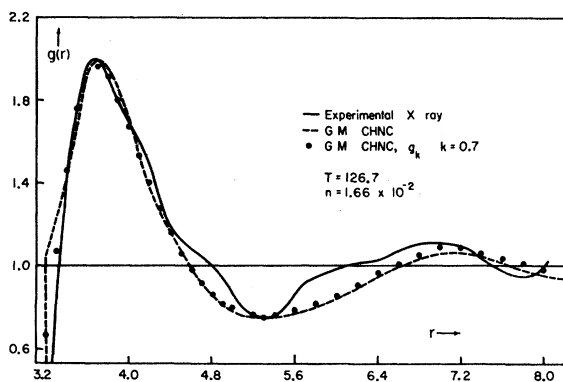
FIG. 32. The dashed curve is the g computed from the CHNC equation with the GM potential. The g_k is shown by the dots. (Maximum value of K used for the computation of g_k is 0.7). The x-ray diffraction curve is due to Eisenstein and Gingrich.

tion we have obtained two solutions which we have called case I and case II. The case I g is very close to the other computed g's, but the case II g is very different from the others (see Fig. 11). It approaches the value $g = 1$ from below. The pressures computed from the g of case I is close to the experimental pressure while the value computed from the g of case II is negative. We consider this solution to be invalid. We expect that a solution corresponding to case II also exists for the LJ potential although we have not been able to find it.

In the case of $T = 149.3°K$ and $n = 4.98 \times 10^{-3}$ particles/Å³, we were unable to obtain any solution for the PY equation with the GM potential. The solution we obtained for the CHNC equation with the GM potential shows the same behavior as the g of case II we discussed above, and we think that this solution is also not good. It also gives negative compressibility.

In Figs. 19 to 31 we have plotted the computed intensities in electron units per atom against K, $(\sin\theta)/\lambda$. The x-ray experimental curves of Eisenstein and
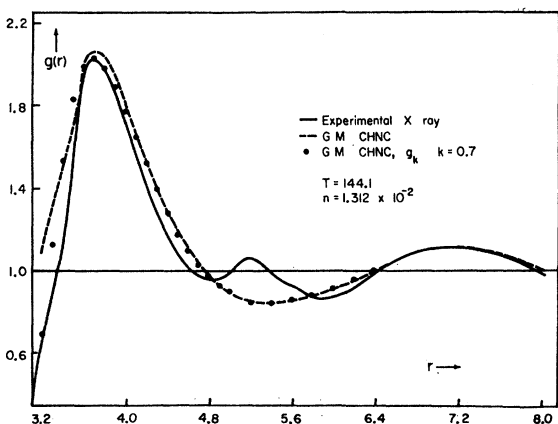

FIG. 33. The dashed curve is the g computed from the CHNC equation with the GM potential. The g_k is shown by the dots. (Maximum value of K used for the computation of g_k is 0.7.) The x-ray diffraction curve is due to Eisenstein and Gingrich.

Gingrich[22] have also been plotted for comparison purposes. It will be seen that the greatest difference between the computed and experimental values occurs at the crests and the troughs of the curves. In some cases the agreement is very good.

It will be seen that the experimental radial distribution curves are not smooth. There are wriggles and bumps on it (see Figs. 11 and 14). In order to see whether these bumps and wriggles can be introduced we have truncated the intensity curves at $K = 0.7$, and then computed g again from the intensity curves. In Figs. 32 and 33 we have plotted the experimental curves, the computed g from the integral equation, and the g which has been computed from the truncated intensity curves. We call this g the g_K for identification. We cut the intensity curves at $K = 0.7$ since the experimental intensity curves which were converted to distribution function form also extended up to $K = 0.7$. It is seen from Figs. 32 and 33 that no wriggles or bumps are introduced in g_K.

Conclusions

In Chap. II we have been able to see the PY and the CHNC equations as two different approximations to an exact integral equation. On the basis of the theory discussed in Chap. II and the comparisons of the results of computations we have been able to draw the following conclusions:

(1) The PY equation is better than the CHNC equation for repulsive potentials, in particular, for the solid spheres.

(2) Both the PY and the CHNC equations are not expected to give good results at high densities.

(3) At low temperature and moderate density, for attractive potentials of the LJ or GM type, the CHNC equation will give better results than the PY equation.

(4) The Guggenheim-McGlashan potential[27] for argon at low temperatures is more realistic than the LJ potential for argon.

(5) In order to obtain better distribution functions at low temperatures for the liquid state of argon, in addition to a better integral equation, a better potential function is also needed.

(6) The CHNC equation with a potential of the LJ or GM type can have more than one solution.

APPENDIX A

The Lennard-Jones and the Guggenheim-McGlashan[9] potentials for argon are given below.

[27] The GM potential can be improved by using Abrahamson's (T.F.D.) [A. A. Abrahamson, Phys. Rev. 130, 693 (1963)] computations for the interatomic potentials for small separations of argon atoms, since Abrahamson's computed values agree closely with the experimently determined values of Amdur and his coworkers [I. Amdur, D. F. Davenport, and M. C. Kells, J. Chem. Phys. 18, 525 (1950); I. Amdur and E. A. Mason, ibid. 22, 670 (1954)].

(i) The LJ potential is given by

$$\mu = 4\epsilon[(a/r)^{12} - (a/r)^6], \tag{A1}$$

where the constants used are

$$\epsilon = 119.76k°K,$$

$$a = 3.405 \text{ Å}.$$

The value of r where the potential energy is minimum is r_0.

$$r_0 = 2^{1/6} \times a = 3.822 \text{ Å}.$$

(ii) The GM potential is given by

$$u(r) = \infty, \quad r < d \tag{A2}$$

$$u(r) = -\epsilon + \kappa \frac{(r-r_0)^2}{r_0^2} - \alpha \frac{(r-r_0)^3}{r_0^3} \frac{(2r_0-r)}{r_0}, \tag{A3}$$

$$r_1 \le r \le r_2$$

$$u(r) = -\lambda\left(\frac{r_0}{r}\right)^6, \quad r \ge r_3. \tag{A4}$$

The constants are

$$\epsilon/k = 137.6 °K; \qquad \kappa/k = 44.9 \times 10^2 °K$$

$$\alpha/k = 19.6 \times 10^3 °K; \qquad r_0 = 3.812 \text{ Å}$$

$$\lambda/k = 150°K,$$

$$d = 3.2 \text{ Å}; \qquad r_1 = 3.6 \text{ Å}$$

$$r_2 = 4.15 \text{ Å}; \qquad r_3 = 5.4 \text{ Å}.$$

The derivatives of the GM potential used in these computations are given below.

$$du/dr = 0, \quad r \le 3.1 \text{ Å}.$$

du/dr is given in the tabular form (Table II) for r lying between 3.2 and 5.4 Å,

$$\frac{du}{dr} = \frac{900 \times (3.812)^6}{r^7} \quad r > 5.4 \text{ Å}.$$

Table II gives the potential function u and its derivatives between 3.1 and 5.4 Å.

TABLE II. The potential function u and its derivatives between 3.1 Å and 5.4 Å.

r (Å)	u (°K)	u'	r (Å)	u (°K)	u'
3.1	∞	0	4.8	−50.50	90.80
3.2	0	−300.00	4.9	−42.50	76.40
3.3	−34.00	−300.00	5.0	−35.50	64.30
3.4	−63.50	−300.00	5.1	−29.50	51.40
3.5	−91.50	−300.00	5.2	−25.00	40.00
3.6	−120.15	−200.00	5.3	=21.50	30.60
3.7	−133.21	−83.00	5.4	−18.56	25.00
3.8	−137.05	−7.57			
3.9	−135.44	−46.39			
4.0	−129.00	81.13			
4.1	−119.78	100.00			
4.2	−110.50	100.00			
4.3	−100.50	100.00			
4.4	−90.50	100.00			
4.5	−80.50	100.00			
4.6	−69.50	100.00			
4.7	−60.00	100.00			

APPENDIX B

In order to compute the pressure, we have used the the Eq. (3.5). For the GM potential equation (3.5) cannot be used in this form since this potential contains a vertical barrier at r equal to d, and at this point ϕ' is discontinuous. The modified equation used for the computation of pressure for the case of GM potential is given by[1,18]

$$\frac{P}{nkT} = 1 - \frac{2\pi n}{3kT}\int \phi' g r^3 dr + \frac{2\pi n}{3}d^3 g(d^+), \tag{B1}$$

where $g(d^+)$ is the value of the distribution function on the right side of the barrier.